The 14-kDa Dynein Light Chain-Family Protein Dlc1 Is Required for Regular Oscillatory Nuclear Movement and Efficient Recombination during Meiotic Prophase in Fission Yeast

**Futaba Miki,* Koei Okazaki,* Mizuki Shimanuki,* Ayumu Yamamoto,†
Yasushi Hiraoka,† and Osami Niwa*‡**

*Kazusa DNA Research Institute, Kisarazu 292-0812, Japan; and †Kansai Advanced Research Center,
Communications Research Laboratory, Kobe 651-2492, Japan

A *Schizosaccharomyces pombe* spindle pole body (SPB) protein interacts in a two-hybrid system with Dlc1, which belongs to the 14-kDa Tctex-1 dynein light chain family. Green fluorescent protein-tagged Dlc1 accumulated at the SPB throughout the life cycle. During meiotic prophase, Dlc1 was present along astral microtubules and microtubule-anchoring sites on the cell cortex, reminiscent of the cytoplasmic dynein heavy chain Dhc1. In a *dlc1*-null mutant, Dhc1-dependent nuclear movement in meiotic prophase became irregular in its duration and direction. Dhc1 protein was displaced from the cortex anchors and the formation of microtubule bundle(s) that guide nuclear movement was impaired in the mutant. Meiotic recombination in the *dlc1* mutant was reduced to levels similar to that in the *dhc1* mutant. Dlc1 and Dhc1 also have roles in karyogamy and rDNA relocation during the sexual phase. Strains mutated in both the *dlc1* and *dhc1* loci displayed more severe defects in recombination, karyogamy, and sporulation than in either single mutant alone, suggesting that Dlc1 is involved in nuclear events that are independent of Dhc1. *S. pombe* contains a homolog of the 8-kDa dynein light chain, Dlc2. This class of dynein light chain, however, is not essential in either the vegetative or sexual phases.

INTRODUCTION

The fission yeast *Schizosaccharomyces pombe* usually propagates in a haploid state. When nutritionally starved, two cells with opposite mating types conjugate and two haploid nuclei fuse to produce a diploid nucleus in a zygote, which is immediately followed by a "zygotic" meiosis. *S. pombe* cells can vegetatively proliferate in a diploid state. When a diploid cell is starved, it can enter into meiosis without conjugation (azygotic meiosis). In the prophase of both types of meiosis, all telomeres cluster near the spindle pole body (SPB) to form a typical chromosomal bouquet, as occurs in many other species (Chikashige *et al.*, 1994, 1997). Loss of a telomere-binding protein, Taz1, impairs the telomere clustering and decreases the frequency of meiotic recombination (Cooper *et al.*, 1998; Nimmo *et al.*, 1998). An SPB-associated protein, Kms1, is also important for the formation of the telomere cluster (Shimanuki *et al.*, 1997; Niwa *et al.*, 2000). *kms1* mutations do not affect mitotic growth, but in the meiotic prophase the SPB tends to disintegrate into a cytoplasmic microtubule organization center (MTOC) and several dots on the nuclear membrane (Shimanuki *et al.*, 1997; Niwa *et al.*, 2000; Shimanuki and Niwa, unpublished data) that contain an SPB protein, Sad1 (Hagan and Yanagida, 1995). Telomeres are often colocalized with the Sad1 dots, and thus the bouquet formation is impaired in the *kms1* mutant; consequently, the meiotic recombination rate is reduced (Shimanuki *et al.*, 1997; Niwa *et al.*, 2000). These and other studies suggest that telomere clustering is a key process for efficient chromosome pairing in fission yeast (reviewed in Hiraoka, 1998; Niwa *et al.*, 2000).

The meiotic prophase nucleus in which telomere clustering is formed is not static. It moves along an oscillatory path with an ever-changing but generally elongated morphology (Chikashige *et al.*, 1994). This movement, often referred to as horsetail nuclear movement, is led by the SPB and requires astral microtubules (Chikashige *et al.*, 1994; Ding *et al.*, 1998). Cytoplasmic dynein is involved in the nuclear movement, because the disruption of the *dhc1⁺* gene, which encodes the

dynein heavy chain, abolishes the movement (Yamamoto et al., 1999). It was recently reported that the nuclear movement is principally led by pulling microtubules that connect the SPB to microtubule-anchoring sites formed on the forward side of the cell cortex with regard to the moving SPB and that cytoplasmic dynein present at the anchoring sites is thought to generate the pulling force (Yamamoto et al., 2001). It is not known, however, how the placement of the dynein molecules is regulated at the anchoring sites.

Cytoplasmic dynein is a multisubunit complex consisting of two heavy chains that contain the motor domain and other associated proteins; that is, intermediate chains, light intermediate chains, and light chains. Various cellular processes, such as vesicular transport, spindle assembly, and nuclear migration, require cytoplasmic dynein, which probably performs its function and achieves its proper localization by selectively using the associated proteins as well as interacting factors such as the dynactin complex (Karki and Holzbaur, 1999). The light chains are represented by 8-, 14-, and 22-kDa proteins (King et al., 1996a,b); the 8- and 14-kDa light chains are also contained in axonemal dynein. The smallest subunit is highly conserved evolutionarily in several species and is required for sensory axon projection and other developmental events in *Drosophila* (Dick et al., 1996; Phillis et al., 1996), nuclear migration in *Aspergillus* (Beckwith et al., 1998), and intraflagellar retrograde transport in *Chlamydomonas* (Pazour et al., 1998). As for the 14-kDa light chain, the mouse gene Tctex-1, one of the candidate factors responsible for meiotic drive (Lader et al., 1989), belongs to this class of proteins (King et al., 1996b). The *Drosophila* homolog dtctex-1 is required for functional sperm (Caggese et al., 2001). The molecular function of the 14-kDa light chain is not understood, except that bovine Tctex-1, but not its homolog RP3, directly binds to the carboxy terminus of rhodopsin and is responsible for the cytoplasmic dynein-dependent transport of rhodopsin vesicles (Tai et al., 1999, 2001). Tctex-1 interacts with the intermediate chain (IC) as well as with other cellular factors (Mok et al., 2001). Tctex-1 and RP3 compete for binding to IC to form different types of cytoplasmic dynein complexes (Tai et al., 2001). Tctex-1 is localized to the Golgi apparatus as well as on cytoplasmic microtubules and on the nuclear membrane in fibroblasts (King et al., 1998; Tai et al., 1998). These findings suggest that the 14-kDa family of proteins has diverse functions.

Investigation of Kms1-interacting proteins by using a yeast two-hybrid system led to the identification of a protein that has homology to the 14-kDa Tctex-1 dynein light chain family proteins. The present results indicate that the Tctex-1 homolog in fission yeast is required for proper localization of Dhc1 molecules to ensure regular oscillatory nuclear movement in the meiotic prophase. We also demonstrate that it has important roles in several processes in the sexual phase, apparently independently of Dhc1.

MATERIALS AND METHODS

S. pombe Strains, Media, and Basic Methods for Genetics and Molecular Biology

The *S. pombe* strains used in this study are listed in Table 1. The media YE, ME, EMM-2, malt-extract broth plus galactose (MEBG), mannose synthetic medium (MSM) as well as experimental methods have been described previously (Moreno et al., 1991; Miyata et

Table 1. *S. pombe* strains used

Name	Genotype
L968	h^{90} wild
L972	h^- wild
SA21	h^{+s} wild
Z310-13D	h^{90} ura4-D18 leu1
F52-3A	h^{90} dlc1::ura4$^+$ ura4 leu1
Z310-10B	h^{90} leu1
Z121-4D	h^{90} kms1::ura4$^+$ ura4 leu1
F71-11D	h^{90} dlc1::ura4$^+$ kms1::ura4$^+$ ura4 leu1
F143-6B	h^{90} dlc1::ura4$^+$ dhc1-d4::ura4$^+$ ura4 leu1
F167-7B	h^{90} kms1::ura4$^+$ dhc1-d4::ura4$^+$ ura4 leu1
F80-1B	h^- ade8 trp1 his5
F63-1C	h^{+s} dlc1::ura4$^+$ ura4 leu1
F84-5A	h^- dlc1::ura4$^+$ ura4 ade8 trp1 his5
F90-1D	h^- dlc1::ura4$^+$ ura4 ura1 lys3
F83-15A	h^{+s} dlc1::ura4$^+$ leu1
HM101	h^- ura1 lys3
F78-18A	h^{+s} fur1 ade6-M210 lys1 leu1
F79-8A	h^- dlc1::ura4$^+$ leu1
F81-2D	h^+ dlc1::ura4$^+$ fur1 ade6-M210 lys1 leu1
F83-2A	h^- dlc1::ura4$^+$
Z439-2A	h^{+s} leu1
F96-2A	h^+ dlc1::ura4$^+$ lys1 leu1
F96-2C	h^- dlc1::ura4$^+$ fur1 ade6-M210
F109-2A	h^+ lys1 leu1
F109-2B	h^- fur1 ade6-M210
F95-1A	h^- dlc1::ura4$^+$ ura1 lys3
F131-1A	h^+ pom1::kan^r leu1
F132-1D	h^+ dlc1::ura4$^+$ pom1::kan^r leu1
F133-1A	h^+ hus2-22
F141-1C	h^+ dlc1::ura4$^+$ hus2-22
F154-4B	h^- ade6-M26 leu1
F155-1D	h^+ ade6-469 leu1
F156-2B	h^- dlc1::ura4$^+$ ade6-M26 leu1
F153-1A	h^+ dlc1::ura4$^+$ ade6-469 leu1
F154-7B	h^{90} ade6-M26 leu1
F156-3A	h^{90} dlc1::ura4$^+$ ade6-M26 leu1
F68-12B	h^{90} dhc1-d2::ura4$^+$ ura4 leu1
F136-15B	h^{90} dhc1-d4::ura4$^+$ ura4 leu1
F73-3A	h^{90} dlc1::ura4$^+$ dhc1::GFP-LEU2 ura4 leu1
MB125	h^{90} dhc1::GFP-LEU2 leu1
F120-23	h^{90} dlc2::kan^r leu1

al., 1997; Okazaki et al., 2000). To observe azygotic meiosis, fresh diploid colonies were isolated for each experiment on a phloxin B-containing YE plate and were checked for efficient azygotic sporulation on an ME plate. The meiotic recombination frequency between chromosomes and a plasmid containing the *ade6-L469* gene inserted into an *LEU2*-based vector pSP1 was measured according to Ponticelli and Smith (1989). To generate DNA fragments to be subcloned, we performed polymerase chain reaction (PCR) by using the primers listed in Table 2. The cloned PCR product sequences were confirmed by DNA sequence analysis. For site-directed mutagenesis, a QuickChange site-directed mutagenesis kit (Stratagene, La Jolla, CA) was used. Probes for filter hybridization were prepared by PCR by using a PCR digoxigenin-labeling mix (Roche Diagnostic, Mannheim, Germany). For Northern hybridization, probes prepared with primers KIP64 and KIP54, and primers PDE17 and PDE18 were used to detect *dlc1*$^+$ and *dhc1*$^+$ mRNAs, respectively. The hybridization signals were detected with antidigoxigenin-alkaline phosphatase conjugate (Roche Diagnostic) and CDP-Star (Tropix, Bedford, MA).

Table 2. Oligonucleotides used

Name	Sequence[a]	Use	Sense/antisense
B23	5′ TCC<u>CCCGGG</u>CCAGGATATGTTAGATAAAGCTCGA 3′		
		Kms1 202 a.a.	(S)
B6	5′ CGC<u>GGATCC</u>TATCAAGAAGGCTGTACCAG 3′		
		Kms1 ~607 a.a.	(A)
pCD35	5′ CTTCTAGGCCTGTACGGAAGTGTTACTTCTGCTCT 3′		
		dlc1+ 5′ PCR and sequence: within pCD vector	
KIP41	5′ CTCCGTCATATTCGGAAGCCTTCAAAACCGGC 3′		
		dlc1+ 5′ PCR and sequence	(A)
KIP42	5′ GCAGCGTGAGCTGCGTGAACGCCTCTAGAAGG 3′		
		dlc1+ 5′ PCR and sequence	(A)
KIP47	5′ GAAGTGGACGATTCGCTGTAAGCG 3′		
		dlc1+ gene colony PCR	(S)
KIP48	5′ GGACGAACACGAATCGTATACACACC 3′		
		dlc1+ gene colony PCR	(A)
KIP56	5′ CG<u>GAATTC</u>TAGTAGCATCTTATGTATCGC 3′		
		dlc1+ gene disruption	(S)
KIP57	5′ GCC<u>CCCGGG</u>TATTTTGATGAGTACAAGG 3′		
		dlc1+ gene disruption	(A)
KIP58	5′ ATC<u>CCCGGG</u>TACCAGTTTTTGC 3′		
		dlc1+ gene disruption	(S)
KIP59	5′ TTTCTGCTCGTTACAACGACG 3′		
		dlc1+ gene disruption	(A)
ura4-4	5′ TGCATACATATAGCCAGTGGG 3′		
		colony PCR: within *ura4*+ gene	(A)
ura4-3	5′ ATGCTCCTACAACATTACCCAC 3′		
		colony PCR: within *ura4*+ gene	(S)
KIP64	5′ GGG<u>GGATCC<u>CAT<u>ATG</u>AGCTGTCCTATAGATTCC 3′		
		dlc1+ Northern probe	(S)
KIP54	5′ AGC<u>GGATCC</u>TTAAATGGAGATCCACATAATGC 3′		
		dlc1+ Northern probe	(A)
KIP63	5′ AGGCC<u>CCGGG</u>C<u>ATATG</u>GAAATGGGGTATTTTGATGAGTACAAGG 3′		
		GFP-tagged Dlc1: ATG → *Sma*I-*Nde*I site	(A)
KIP64	5′ GGG<u>GGATCC</u><u>CATATG</u>AGCTGTCCTATAGATTCC 3′		
		GFP-tagged Dlc1: ATG → *Sma*I-*Nde*I site	(S)
cGFP-5′	5′ GG<u>AATTC</u>C<u>ATAT</u>GAGTAAAGGAGAAGAACTTTTCAC 3′		
		GFP-tagged Dlc1: within GFP	(S)
cGFP-3′	5′ ACGG<u>CCCGGG</u>ACCTTTGTATAGTTCATCCATGC 3′		
		GFP-tagged Dlc1: within GFP	(A)
PDH1	5′ GCTGTCCCCTTAAACCCGTTCATTGC 3′		
		dhc1+ Northern probe	(S)
PDH4	5′ TTCCCTGAACCTGTCTTGCCTAGCAG 3′		
		dhc1+ Northern probe	(A)
PDE17	5′ GGG<u>GATTCC</u><u>ATATG</u>GCAGTCATCAAGGC 3′		
		dlc2+ Northern probe and GFP-tagged Dlc2	(S)
PDE18	5′ ACGC<u>GGATCC</u>TAACCAGACTTGAACAG 3′		
		dlc2+ Northern probe and GFP-tagged Dlc2	(A)

[a] Recognition sequences of restriction enzymes are underlined. The initiation codon or termination codons are double-underlined.

Two-Hybrid System

A commercially supplied yeast two-hybrid system (Matchmaker two-hybrid system 2; CLONTECH, Palo Alto, CA) was used according to the manufacturer's protocol. A bait plasmid containing a segment of Kms1 protein (amino acid residues 202–607) fused to the Gal4 DNA-binding domain (Gal4BD) in pAS2.1 was used to screen an *S. pombe* cDNA library constructed with pGAD GH (CLONTECH). Various parts of Kms1 protein as well as Dlc1 were fused to the activation domain on pACT2 by using PCR-generated fragments. In some cases, the termination codon was introduced by site-directed mutagenesis. Table 2 lists the primers used in the study.

Preparation of Anti-Dlc1 Antiserum and Western Blotting

The glutathione-S-transferase (GST)-fused Dlc1 protein was produced in *Escherichia coli* then purified and the GST moiety was removed. Dlc1 protein thus prepared was used to immunize rabbits. To express Dlc1 in *E. coli*, the open reading frame (ORF) of *dlc1*+ cDNA was amplified by PCR with primers KIP64 and KIP54 and inserted into the *Nde*I/*Bam*HI site of pET3a (Novagen, Darmstadt, Germany). For Western blot, rabbit anti-Dlc1 antiserum and rabbit anti-Sad1 antibody (Okazaki *et al.*, 2000) were used. Dlc1 was separated on 20% SDS-PAGE with high-molarity buffers (Okajima *et al.*, 1993) and detected using horseradish peroxidase-conjugated don-
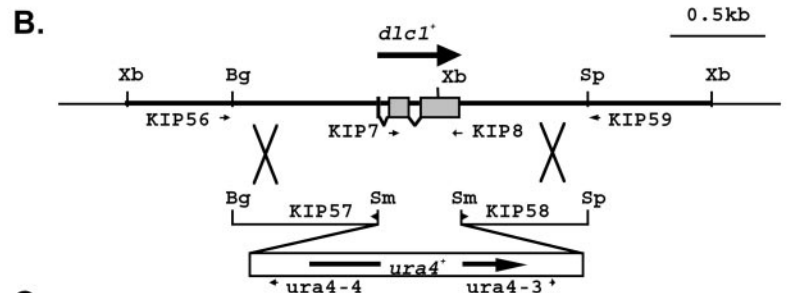
Figure 1. *dlc1+* gene and its product. (A) Nucleotides and the predicted amino acid sequences of the *dlc1+* are shown. The nucleotide sequence of a full-length cDNA is shown in uppercase and the other genomic sequences, including two presumed introns, are shown in lowercase. The in-frame initiation codons upstream of the first nucleotide of the cDNA are boxed. The 5' ends of the longest and shortest cDNAs obtained by the yeast two-hybrid screening are double underlined. The segment between the two arrowheads was replaced by the *ura4+* gene cassette for gene disruption. (B) Scheme for gene disruption of the *dlc1+* gene. The positions and directions of the primers are indicated by small arrows. Restriction sites shown are *Xba*I (Xb), *Bgl*II (Bg), *Spe*I (Sp), and *Sma*I (Sm). (C) Homology of Dlc1 with the 14-kDa dynein light chain family. Amino acid sequence of *S. pombe* Dlc1 is aligned with *D. melanogaster* Tctex1 (Y08968), *Homo sapiens* Tctex1 (U56255), *Anthocidaris crassispina* sperm flagellar outer-arm dynein LC3 (AB004251), *Chlamydomonas reinhardtii* inner arm dynein light chain Tctex1 (AF039437), *H. sapiens* rp3 (U02556), and *Caenorhabditis elegans* T05C12-5 ORF (Z66500). Amino acids identical among more than four proteins are shaded in black and amino acids of conservative changes are shaded in gray.

key anti-rabbit secondary antibody (Amersham Biosciences, Piscataway, NJ) and Renaissance Western Blot Chemiluminescence Reagent Plus (PerkinElmer Life Sciences, Boston, MA). *S. pombe* total protein was prepared by the alkaline extraction method (Silve *et al.*, 1991; Tange *et al.*, 1998).

Cloning of dlc1+ and dlc2+ Genes

Using an *S. pombe* cosmid library (Mizukami *et al.*, 1993), we cloned the *dlc1+* gene (from cosmid c1805) and the *dlc2+* gene (c926). A *Hinc*II-*Spe*I fragment containing the *dlc1+* gene was subcloned into the *ars1/LEU2*-based vector pALSK+ (Tanaka *et al.*, 2000) to generate the plasmid pSD15. A *Hin*dIII fragment containing the *dlc2+* gene was also cloned in this vector. The start codon in the *dlc1+* gene was determined by sequencing the PCR product amplified from a full-length cDNA library (Tanaka *et al.*, 1999) with primers pCD35 and KIP41 or KIP42. The sequence of seven independent fragments contained cDNA with identical 5' end, suggesting that they represented the full-length cDNA. The nucleotide sequence of the full-length *dlc1+* cDNA was deposited with the accession number

AF196291. We first obtained a partial cDNA sequence for Dlc2 by using degenerate oligonucleotide primers designed from the conserved amino acid sequences among the 8-kDa light chain proteins (Beckwith *et al.*, 1998) and then cloned a full-length cDNA sequence (deposited with the accession number AF197476). There were four introns in the *dlc2+* gene.

Gene Disruption

To disrupt the *dlc1+* gene (Figure 1B), the upstream region from the start codon and the downstream region from the termination codon were amplified using pairs of primers, KIP56/KIP57 and KIP58/KIP59, and digested with *Eco*RI and *Sma*I and with *Sma*I and *Spe*I, respectively. These two fragments and *Eco*RI/*Spe*I-digested pBluescriptII were three-piece ligated. The resulting plasmid (pSD19) had the sequence of the *Sma*I site, in place of the *dlc1+* coding sequence, to be inserted by the *S. pombe* *ura4+* gene cassette. The 1.8-kb *Hin*dIII fragment of the *ura4+* gene was blunt-ended and inserted into the *Sma*I site of pSD19 to generate the pSD26 plasmid. The *Bgl*II-*Spe*I fragment of pSD26 containing *ura4+* was introduced into Z310-13D

(h^{90} *ura4-D18 leu1*). Stable Ura$^+$ transformants were analyzed by PCR and Southern hybridization to verify correct gene disruption. To disrupt the ORF of the *dlc2$^+$* gene with the G418-resistant marker, the PCR-based gene targeting method was used (Bähler *et al.*, 1998).

Construction of a Plasmid Expressing Green Fluorescent Protein (GFP)-tagged Dlc1

A 0.7-kb fragment in the upstream region of the start codon was amplified using primers KIP56 and KIP63, and the entire Dlc1 coding region, except for the first intron, was amplified with KIP64 and KIP59, respectively, from relevant parts of genomic DNA. These amplified fragments were digested with *Eco*RI and *Sma*I and with *Sma*I and *Spe*I, respectively, and ligated to *Eco*RI/*Spe*I digested pBluescriptII to construct plasmid pSD29. The coding sequence of GFP with improved fluorescence (Craven *et al.*, 1998) was amplified by PCR with primers cGFP-5′ and cGFP-3′, digested with *Nde*I and *Sma*I and inserted into pSD29 digested with the same restriction enzymes. The *Eco*RI-*Spe*I fragment containing the GFP-Dlc1 fusion gene was subcloned into pALSK$^+$ to construct plasmid pSD38.

Microscopy

Microscopic observation was performed using the Delta Vision microscope system (Applied Precision, Issaquah, WA), which allows for multicolor and three-dimensional acquisition of digitized images. For fixed cells, several Z-axis sections at 0.1-μm intervals were combined using a quick projection program. Computational removal of out-of-focus signals was not performed unless otherwise noted. For time-lapse observation of live cells, cells scraped from an agar plate were suspended in 1 μg/ml Hoechst 33342 and incubated for 5 min. Cells were collected by centrifugation, suspended in MSM medium containing 1 μg/ml Hoechst 33342, and placed onto a thin film of 2% agarose gel. The film was sandwiched with coverslips and placed on the stage. Each set of images for GFP and Hoechst 33342 were obtained with a 2-s exposure of 490 nm (neutral density filter 10%) and 0.2-s exposure of 380-nm excitations, respectively, at 25–26°C. The colors in the merged images for each wavelength in this report are all artificial.

Observation of Cells Expressing GFP-tagged Proteins

The pSD38 plasmid was introduced into *S. pombe* strains Z310-10B, F136-15B, Z121-4D, and F52-3A to observe GFP-Dlc1. To visualize microtubules, Z310-10B, F52-3A, and F136-15B, F143-6B were transformed with pDQ105, a multicopy plasmid that carried GFP-α-tubulin fusion gene (GFP-*atb2$^+$*), which was placed under the *nmt1* promoter (Ding *et al.*, 1998) and cultivated on an EMM2 plate containing 10 μM of thiamine to allow limited expression of the fusion gene. The strain in which the *dhc1$^+$* gene was removed but expressing the GFP-tagged Dhc1 (Yamamoto *et al.*, 1999) was crossed with appropriate strains to obtain F73-3A and MB125 (Table 1). These strains were cultivated on YE plates. Cells were induced into meiosis by placing them at high density on an ME plate for 6–12 h at 26°C.

Laser Photobleaching of GFP-labeled Microtubules

GFP-labeled microtubules were photobleached and observed on a DeltaVision microscope system in a temperature-controlled room (Haraguchi *et al.*, 1997, 2000); experiments were performed at 26°C. For photobleaching, a nitrogen laser-pumped dye laser, Micropoint Laser System (Photonic Instrument, Arlington Heights, IL), was equipped on the DeltaVision microscope system, which was modified to remove an optical fiber illumination module, and Coumarin 440 (440-nm emission light) was used as the laser dye. The laser beam was focused ~1 μm below the coverslip surface; the illumi-

nated area for the photobleaching had an approximate diameter of 1 μm in the focal plane. GFP-labeled microtubules were exposed to a single pulse of the laser beam. The dynamics of the GFP-labeled microtubules was recorded on the DeltaVision microscope as described previously (Yamamoto *et al.*, 1999, 2001). An Olympus 60×/1.4 numerical aperture PlanApo oil immersion objective lens was used for photobleaching and the following observation.

Immunofluorescence Staining and Fluorescence In Situ Hybridization

Cells were fixed with 3% formaldehyde and 0.2% glutaraldehyde. Immunostaining and in situ hybridization were performed as described previously (Okazaki *et al.*, 2000). TAT1 mouse monoclonal anti-α-tubulin antibody and the anti-Sad1 antibody were used to stain microtubules and SPB, respectively. The secondary antibodies were Cy5-conjugated donkey anti-mouse antibody (Amersham Biosciences) and Cy3-conjugated goat anti-rabbit antibody (Jackson Immunoresearch Laboratories, West Grove, PA). DNA was stained with 1 μg/ml 4′,6-diamidino-2-phenylindole (DAPI). The probes for fluorescence in situ hybridization were labeled with Cy3-conjugated or Cy5-conjugated dCTP (Amersham Biosciences). Cosmid cos212 (Funabiki *et al.*, 1993) and plasmid YIp10.4 (Toda *et al.*, 1984) were used for the subtelomeric repeated sequence of chromosomes I and II, and the rDNA repeat at the telomere-proximal regions of chromosome III, respectively.

RESULTS

Identification of a Protein Showing Homology with a Dynein Light Chain

We screened an *S. pombe* cDNA library by using the yeast two-hybrid system to identify cellular factors that interact with Kms1. Using the carboxy-terminal two-thirds of the Kms1 protein (amino acid sequence 202–607) as bait, we identified four kinds of proteins (Miki, Shimanuki and Niwa, unpublished data). The amino acid sequence of one of the proteins was similar to the 14-kDa dynein light chain family (Figure 1). It was most similar to *D. melanogaster* Tctex1 (25% identity and 49% similarity). Although the overall similarity to other Tctex-1 family proteins was not as high, the results obtained in the present study indicate that it is closely related to cytoplasmic dynein, hence we designated the gene *dlc1$^+$*.

Characterization of dlc1$^+$ Gene

The *dlc1$^+$* gene was cloned by colony hybridization and sequenced (Figure 1A). In the genomic sequence, two additional in-frame ATG codons and therefore larger ORFs exist (Figure 1A). To determine the start codon, we sequenced full-length cDNAs obtained from another *S. pombe* cDNA library. None of the cDNAs contained the upstream ATG codons (Figure 1A). To verify the protein-coding sequence, the polypeptide with 111 amino acids encoded by the *dlc1$^+$* cDNAs was expressed in *E. coli* and compared with endogenous *S. pombe* Dlc1 protein in a Western blot by using anti-Dlc1 antiserum. Both proteins produced a single band that migrated to the same position (Figure 2A). The band was missing when an extract from *dlc1*-deleted cells (see below) was used, indicating that the antibody was specific for Dlc1 protein (Figure 2A). No extra bands were produced from extracts of cells in the sexual phase (Figure 2B). Thus, we concluded that the *dlc1$^+$* gene encodes the 111 amino acids, with a calculated
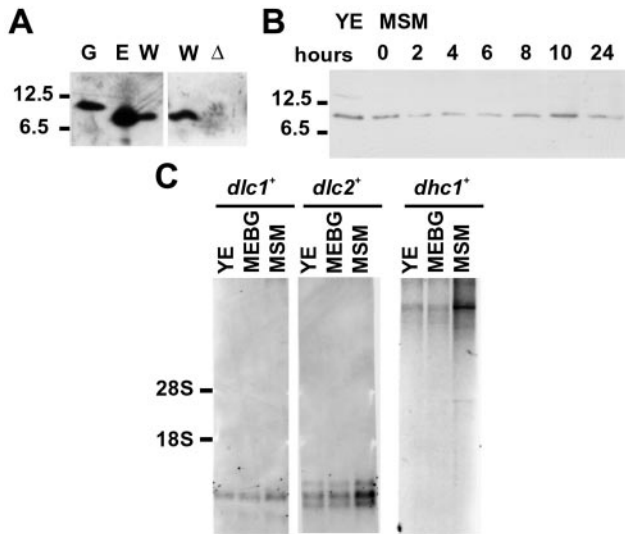
Figure 2. Identification and expression of Dlc1. (A) Western blot analysis by using anti-Dlc1 antiserum. Purified Dlc1 protein with an additional seven amino- and nine carboxy-terminal sequences used for immunization (G), total protein of *E. coli* expressing the *dlc1*+ cDNA (E), total protein of exponentially growing wild-type fission yeast (Z310-10B) (W) or of *dlc1*Δ (F52-3A) cells (Δ) were separated on 20% SDS-PAGE. The positions of protein standards are shown on the left. (B) Expression level of Dlc1 protein detected by Western blot. Wild-type strains L972 and SA21 were induced to conjugate in MSM and total cell extracts from the same number of cells were prepared at the indicated times. Cells began to aggregate, conjugate, and sporulate at 6, 8, and 24 h, respectively. A control sample from exponentially growing L972 in YE was run in the left lane. (C) Northern blot hybridization with a *dlc1*+, *dlc2*+, or *dhc1*+ probe. Total RNA (20 μg) from wild-type homothallic strain L968 cells was loaded in each lane. RNA was extracted from cells growing exponentially in a rich medium (YE), in a poor medium (MEBG), or from cells in a conjugation medium (MSM) (38% of cells were conjugated, and among the zygotes, 30% were under the karyogamy and 70% were in the horsetail phase to meiosis I). The positions of rRNAs are shown on the left.

molecular mass of 12.3 kDa, although it was not ruled out that a minor fraction of the gene expression might be from the larger ORFs. Note that Dlc1 protein migrated at ~9 kDa in the SDS-polyacrylamide gel (Figure 2A). However, a bacterially produced Dlc1 with extra 16 amino acid residues (calculated molecular weight 13.6) migrated at 10.5 kDa (Figure 2A, lane G), indicating that the apparent discrepancy between the migrating position in the gel and the calculated values was probably not due to an unusual start site. The dynein heavy chain (Dhc1) is only detectable during karyogamy through early meiosis (Yamamoto *et al.*, 1999). Consistently, the *dhc1*+ mRNA was massively induced during the sexual phase and the gene expression remained very low in vegetatively proliferating cells (Figure 2C). In contrast, such massive induction was not observed for the *dlc1*+ gene, although expression might be slightly increased during the sexual phase as shown by both Northern hybridization and Western blotting (Figure 2, B and C).

Disruption of *dlc1*+ Gene

A DNA fragment in which the whole ORF of the *dlc1*+ gene was replaced with a *ura4*+ gene cassette was used for transformation of a homothallic haploid strain (Figure 1B). Correct disruption of the gene was verified both by PCR and Southern hybridization. The *dlc1*-disruptant (*dlc1*Δ) had no discernible defect in the vegetative growth phase. The morphology and positioning of dividing nuclei were normal, based on DAPI staining. The length of the cells with the dividing nuclei was not different from that of wild-type cells. One peculiar feature we noted was that the doubling time of *dlc1*Δ mutants was slightly shorter than the wild-type with otherwise the same genotype, the reason for this is not known. In the sexual phase, however, the mutant had several defective phenotypes in nuclear movement, meiotic recombination, karyogamy, sporulation, and chromosome rearrangement as shown below.

Impaired Nuclear Movement in *dlc1*Δ Mutant during Meiotic Prophase

The *dhc1* mutant lacks the oscillatory nuclear movement that normally occurs during prophase in wild-type meiosis (Yamamoto *et al.*, 1999). Given the homology of Dlc1 with dynein light chain, we investigated the effect of the *dlc1*-null mutation on nuclear movement. Because the nuclear movement is led by the SPB that serves as the MTOC, we traced the MTOC in live cells containing GFP-labeled microtubules. The paths of the observed MTOC were projected on a plane as shown in Figure 3. Consistent with a previous report (Yamamoto *et al.*, 1999), in both zygotic (Figure 3, top) and azygotic (Figure 3, bottom) meiosis, horsetail movement was almost absent in the *dhc1-d4* mutant, although there were occasional apparently random movements.

In the *dlc1*Δ mutant, the horsetail movement was also impaired, but apparently not as severely as in the *dhc1* mutant. The profiles of the MTOC paths in *dlc1* mutant cells differed from each other; nevertheless, some common features could be drawn from these profiles. First, an important feature was that when the MTOC moved, its speed often reached up to 70% of the highest speeds observed in wild type. Second, there were phases in which the MTOC slowed down or was wandering. In extreme cases, the wandering appeared to last almost throughout the prophase (Figure 3, right-most cell in azygotic meiosis). To express these features in a quantitative manner, we plotted the length of the MTOC path in 5-min intervals (Figure 4A). The average number of movements >10 μm during a 2-h observation period were 2.1 and 14.3 in the *dlc1* mutant and wild type, respectively, indicating a shorter duration of the fast-moving phases in the mutant. In the *dhc1* mutant, there were no movements >5 μm. Third, the regulatory mechanism for switching the direction of nuclear movement appeared to be impaired in the *dlc1* mutant. The MTOC in the mutant did not follow the regular oscillatory path that occurs in wild-type cells. Another feature was that in the wandering phase, the motion of the MTOC was faster than the *dhc1* mutant. Thus, abnormal behavior of the MTOC was basically similar in both zygotic and azygotic meioses.

We then examined a *dhc1*Δ *dlc1*Δ double mutant to determine whether the MTOC movement in the *dlc1* single mutant was dependent on dynein activity. The defect in the MTOC
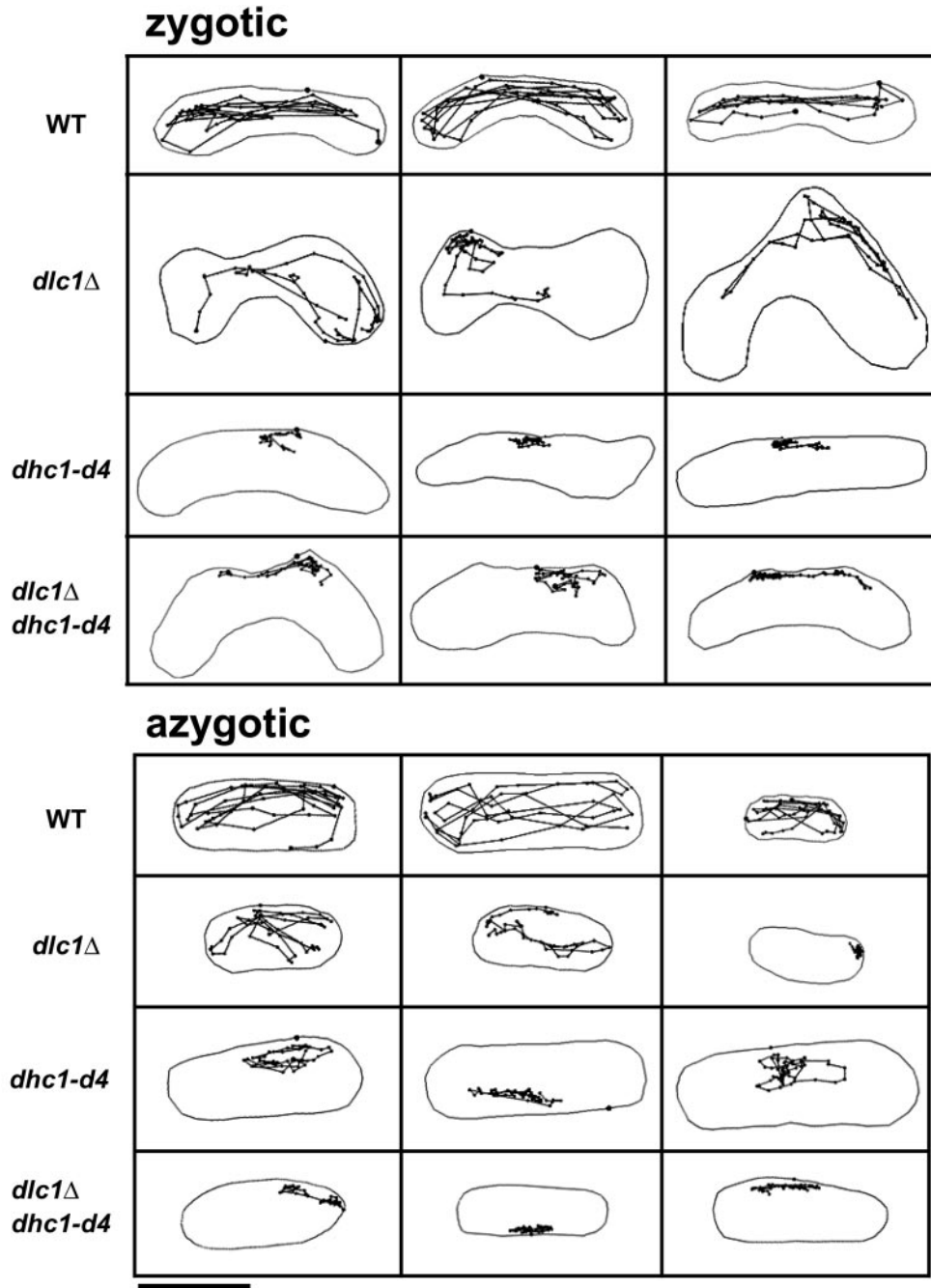
zygotic

azygotic

Figure 3. Paths of the SPB/ MTOC movement during meiotic prophase. Z310-10B (WT), F52-3A (*dlc1Δ*), F136-15B (*dhc1-d4*), and F143-6B (*dlc1Δ dhc1-d4*) were transformed with pDQ105 and zygotic and azygotic meioses were observed in live cells. Images of GFP-α-tubulin for microtubules and of Hoechst 33342 for DNA were taken every 30 s. The position of the MTOC in each image was projected to a single plane and connected with thin lines.

movement in zygotic as well as in azygotic meioses of the double mutant was indistinguishable from that in the *dhc1* single mutant (Figures 3 and 4A). This result indicates the MTOC movement in the *dlc1* mutant is dependent on Dhc1.

Abnormal Cytoplasmic Microtubule Arrays in Mutant

Because cytoplasmic microtubules mediate horsetail movement (Ding *et al.*, 1998; Yamamoto *et al.*, 2001), we observed microtubule arrays formed in the *dlc1* mutant with respect to the direction of the MTOC movement, by using GFP-tagged α-tubulin. When cells with a moving SPB were arbitrarily chosen for observation, in one-third of the wild-type meioses (22/66), only microtubule(s) extending forward from the SPB were clearly visible (Figure 5), but such a conformation was never observed (0/68) in the *dlc1* mutant. Instead, in 20 of 68 meioses in the mutant, prominent microtubules extending rearward with wide angles were observed but forward-extending microtubules were faint or missing (Figure
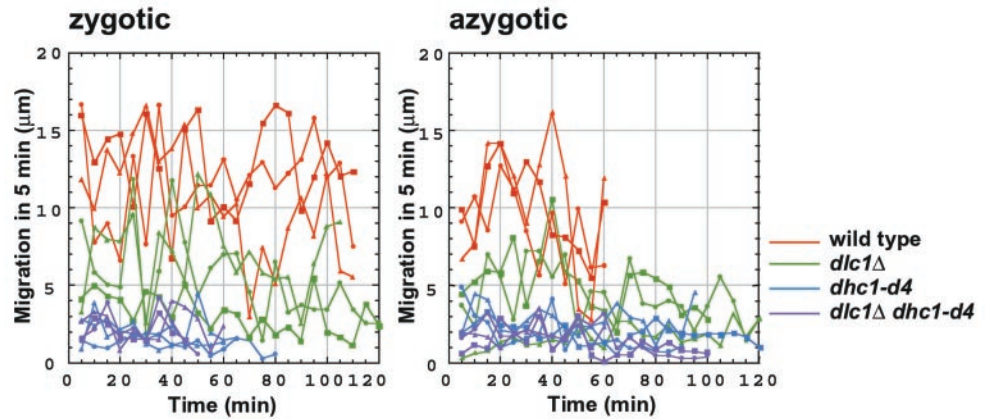
Figure 4. Length of the MTOC path measured at 5-min intervals from the data shown in Figure 3.

5). This type of microtubule was rarely observed (2/66) in wild type. For this observation, only one focal image was acquired at each time point (and therefore no computational image processing was applied), so that nonbundled microtubules might have been overlooked. Nevertheless, it was evident that cytoplasmic microtubule arrays formed in the *dlc1* mutant were very different from those in wild type. Particularly, forward-extending microtubules, which paralleled the long axis of the cell and were apparently pulling the MTOC, were missing in the *dlc1* mutant.

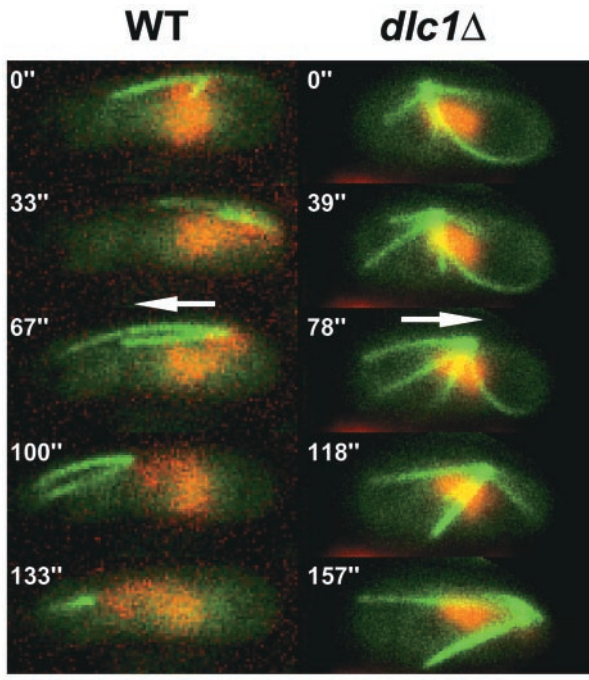To more closely examine microtubule dynamics in the mutant, we performed a time-lapse and optical multisection

Figure 5. Typical astral microtubule array formed in the prophase of a zygotic meiosis in strains with indicated genetic background. Arrows indicate the direction of SPB movement. Each image was acquired at the indicated time. Bars, 5 μm.

observation of GFP-labeled microtubules with a minimal interval between each image acquisition. This allowed us to continuously follow the behavior of microtubule ends. Photobleaching of a microtubule segment was simultaneously performed, thus it was possible to determine at which end assembly/disassembly of microtubules took place. Previous experiments indicated that microtubule assembly and disassembly occurred only at the microtubule ends distal to the SPB both in wild type and in the *dhc1* mutant (Yamamoto *et al.*, 2001). This was also the case in the *dlc1* mutant, because the distance from the bleached segment to the SPB did not change in any of the 75 cells analyzed, irrespective of whether the treated microtubules were lengthening or shortening or of the direction the SPB was moving (Figure 6). We then examined the behavior of the distal ends with regard to the direction of SPB movement. The distal ends could be fixed in position on the cell cortex or unfixed (touching or apparently not touching to the wall). Three cells with a MTOC moving at relatively high speeds (>2 μm/min) were chosen for analysis (one example is shown in Figure 6B). The number of microtubules on each side of the cell and the state of the microtubules (fixed or unfixed, lengthening or shortening) were changing with time, and the results are shown as the cumulative number of microtubules of each category obtained from a total of 49 time points (Figure 6C). As shown in Figure 6C (left), microtubules extending backward with their distal ends fixed on the cell cortex were almost always present when the MTOC was moving (Figure 6B, microtubules A–D). Such microtubules were lengthening, and therefore, appeared to be pushing the SPB. In contrast, fixed microtubules extending forward were rare. The only exceptional case in this analysis was microtubule E in Figure 6B. This microtubule was shortening more or less in conjunction with the SPB movement. It was not certain, however, whether the microtubule was engaged in pulling the SPB, judging from the orientation of the microtubule to the direction of SPB movement. For instance, in the 96-s frame in Figure 6B, the microtubule appeared to be bent due to a pushing force from the SPB. As for unfixed microtubules, they were present on both sides of the cell, although there were relatively fewer shortening microtubules on the backward side (Figure 6C, middle and right). Thus, it was likely that the nuclear
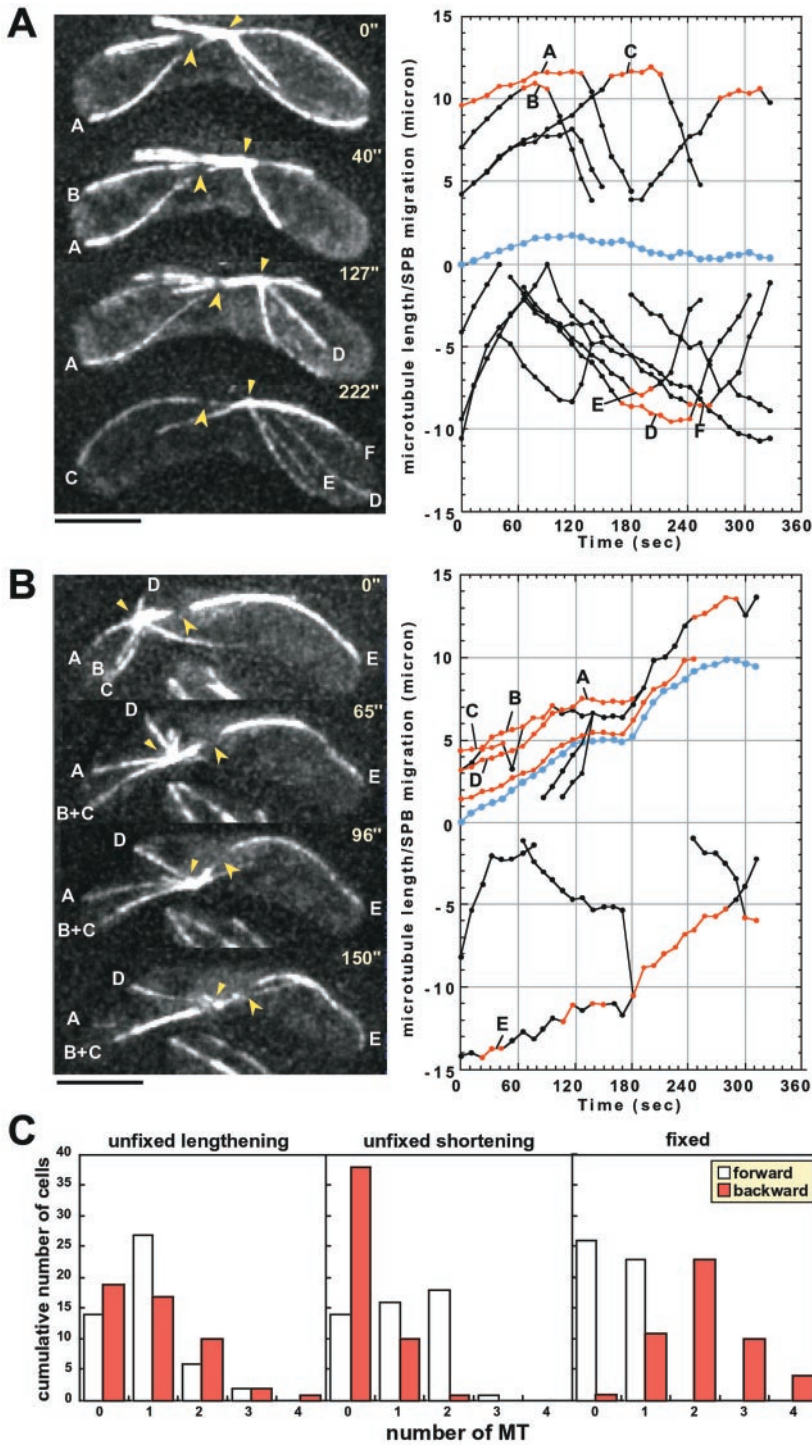
Figure 6. Microtubule dynamics in the *dlc1* mutant. (A and B) Processed images at the time indicated in seconds are shown. Small arrowheads, MTOC; large arrowheads, photobleached segments. The lengths of the microtubules, marked with letters, were measured. Bars, 5 μm. In the graphs, the lengths of individual microtubules are plotted against time. Negative values indicate that microtubules are extending rightward. Segments of lines shown in red indicate that the distal tip is fixed in position on the cell cortex. Blue lines in the middle indicate the position of the MTOC, the upper side being the right side in the pictures. (C) Three zygotes with an SPB moving at a speed of >2 μm/min were chosen and the number of microtubules in each category (fixed or unfixed, lengthening or shortening) of each cell was scored at 49 time points. Cumulative number of each type of microtubule is shown in the histograms.

movement in the *dlc1* mutant was driven, at least partially, by a pushing force from the backward-extending microtubules. This appeared to also be true for slower moving MTOCs analyzed in eight cells (Figure 6A). Microtubules A and D in Figure 6A, when fixed, were lengthening in a well-coordinated manner with the SPB movement, but none were fixed and shortening. The rate of elongation of unfixed microtubules was 3.7 ± 0.9 μm/min (n = 34), which was very similar to that previously obtained for microtubules in elongation phase in wild-type cells (Yamamoto *et al.*, 2001). On the other hand, the rate of shortening of unfixed microtubules was 6.8 ± 3.2
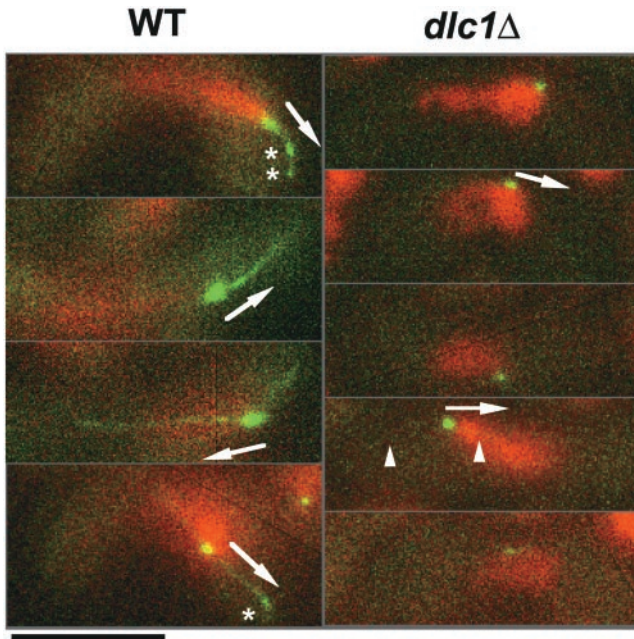
Figure 7. Reduction in localized GFP-Dhc1 in meiotic prophase nuclei in the *dlc1Δ* mutant. Strains MB125 (WT) and F73-3A (*dlc1Δ*) were observed without fixation. Representative images obtained from different cells are shown. Green, GFP-Dhc1; red, DNA. Arrows indicate the direction of nuclear movement. Asterisks indicate presumed microtubule anchors on the cell cortex; arrowheads indicate GFP signals along cytoplasmic microtubules in the *dlc1* mutant. Bar, 5 μm.

μm/min (n = 25). This value was also similar to that measured in wild-type cells where the SPB was not moving continuously but wandering near the ends of the cell (Yamamoto *et al.*, 2001).

Localization of Dhc1 in dlc1 Mutant

We then investigated the localization of Dhc1 in the *dlc1* mutant and found that Dhc1, which was tagged with GFP (Yamamoto *et al.*, 1999), was still present at the SPB, although the signal intensity was significantly reduced compared with wild type (Figure 7). Only occasionally was a faint fluorescent signal observed along the microtubules (Figure 7, arrowheads). Furthermore, Dhc1 signals on the cell cortex were almost invisible in the mutant. Thus, the loss of Dlc1 abolished the placement of Dhc1 to the microtubule anchors, which would be formed on the forward side of the cortex (Yamamoto *et al.*, 1999, 2001; Figure 6, asterisks in wild type). The forward-extending microtubules in wild-type cells are linked to the cell cortex at anchoring sites and are required for normal nuclear movement (Yamamoto *et al.*, 1999, 2001). The localization and intensity of fluorescence of GFP-Kms1 (Tange *et al.*, 1998) were not affected by the *dlc1* mutation in either vegetative or meiotic cells (our unpublished data).

Localization of Dlc1

To analyze the localization of Dlc1, GFP was fused to the amino terminus of Dlc1. The fusion protein was expressed

under the *dlc1+* promoter on a multicopy plasmid. The expression level of the GFP-Dlc1 in wild-type cells was approximately twice that of the endogenous Dlc1 as estimated in a Western blot with an anti-Dlc1 antibody. This GFP-Dlc1 fusion protein was functional because the plasmid could rescue the sporulation abnormality of *dlc1Δ* cells (our unpublished data). In live cells expressing the fusion protein, GFP signals were most prominently observed at the leading tips of horsetail nuclei but there were also signals along cytoplasmic microtubules as well as at sites on the cell cortex (Figure 8A). The fluorescence at the leading tips overlapped with the anti-Sad1 staining (Figure 8B). Such a localization pattern was almost identical with that of GFP-Dhc1 (Yamamoto *et al.*, 1999), except that the Dlc1 signals on the cortex were less prominent compared with Dhc1. The most remarkable difference between these proteins was that Dlc1 was present at the SPB not only during the sexual phase when Dhc1 was present (Yamamoto *et al.*, 1999) but also during the vegetative phase as well as in a later phase of meiosis when there was little or no Dhc1 (Figure 8B). Consistently, Dlc1 in vegetative cells was localized at the SPB in the *dhc1-d4* mutant at a level comparable with that in wild-type cells (our unpublished data). The vegetative localization of GFP-Dlc1 was also not affected by the *kms1* mutation (our unpublished data), indicating that Dlc1 localization at the SPB during vegetative phase does not require Kms1 or Dhc1. Dlc1 was also localized at the SPB/MTOC in both *dhc1* and *kms1* mutants during meiotic prophase, although there might be less protein than in wild type (Figure 8A). There was very little, if any, Dlc1 on the cell cortex in the dhc1-d4 mutant. In the *kms1* mutant, Dlc1 was not detected on the Sad1-containing nuclear dots that are characteristically produced in this mutant (Niwa *et al.*, 2000; Shimanuki, unpublished data).

Reduction of Meiotic Recombination in dlc1Δ Mutant

We performed a tetrad analysis of zygotic asci to determine recombination frequencies in several chromosomal regions (Table 3). The frequencies were reduced 5.6- to 16.8-fold in the *dlc1* mutant compared with those in wild-type cells. These values were comparable with those previously determined in *kms1-1* and *dhc1Δ* mutants (Shimanuki *et al.*, 1997; Yamamoto *et al.*, 1999). Importantly, recombination rates between plasmids and chromosomes were only mildly affected by the *dlc1* mutation as measured by the frequency of an intragenic recombination between *ade6-M26* and *ade6-469* (Table 4). Thus, Dlc1 appeared to have a role in the spatial arrangement of homologous chromosomes to ensure efficient meiotic recombination.

The effect of *dhc1* mutations on recombination in zygotic meiosis was different from that in azygotic meiosis (Yamamoto *et al.*, 1999). In wild-type cells, recombination in azygotic meiosis is generally less frequent compared with zygotic meiosis (Yamamoto *et al.*, 1999). In *dhc1Δ* strains, however, it is almost reversed, because *dhc1* mutations greatly interfered with recombination in zygotic meiosis, whereas the effect was mild for azygotic meiosis. We compared the two types of meiosis in the *dlc1Δ* mutant by using the recombination frequency between *ade6* and *fur1* loci with a random spore method. The *dlc1*

Figure 8. Localization of GFP-Dlc1. (A) GFP-Dlc1 plasmid was introduced into Z310-10B (WT), F136-15B (*dhc1-d4*), and Z121-4D (*kms1Δ*), and live zygotes were observed at the indicated intervals. Chromosomes, red; GFP-Dlc1, green, also in black-and-white images on the right side of each merged image. (B) Z310-10B cells containing GFP-Dlc1 in the vegetative phase (left) and in the sexual phase (right) were fixed and stained with DAPI, anti-Sad1 antibody, and anti-tubulin TAT1 antibody simultaneously. Merged: blue (DNA), green (GFP-Dlc1), red (Sad1), and white (microtubule). Bars, 5 μm.

mutation had almost the same differential effect on zygotic and azygotic meioses as the *dhc1* mutant (Table 5). Recombination frequency was further reduced when both of these genes were mutated (Table 5), indicating that the roles of these genes in recombination might not overlap completely. Note that the double mutant had a severe karyogamy defect, as described below, so the apparently greater reduction in recombination in zygotic meiosis might be due to the presence of spores produced from unfused nuclei.

Relocation of rDNA toward SPB Was Impaired in dlc1 Mutant

We examined the effect of the *dlc1Δ* mutation on clustering of telomeres beneath the SPB during the meiotic prophase by fluorescence in situ hybridization by using cos212 probe for telomeres of chromosomes I and II and an rDNA probe for telomeres of chromosome III. Consistent with previous reports, in almost all wild-type nuclei, telomeres made a single cluster in both zygotic and azygotic meioses (Figure 9

Table 3. Tetrad analysis of genetic linkage in *dlc1Δ*
  Spores formed in zygotic asci were analyzed for the linkage of two genetic markers indicated.

Genetic markers	Cross[a]	No. of tetrads			Genetic distance	
		PD[b]	T[c]	NPD[d]	Total	cM
ura1-lys3	w × w[e]	72	44	1	117	21.4
	Δ × w[f]	72	40	3	115	38.3
	w × Δ[g]	72	28	0	100	14
	Δ × Δ[h]	108	7	0	115	3
ura1-pom1	w × w[i]	94	27	2	123	15.9
	Δ × Δ[j]	117	2	0	123	2.4
ura1-hus2	w × w[k]	126	35	3	164	16.2
	Δ × Δ[l]	301	17	2	320	4.5
leu1-his5	w × w[m]	42	38	1	81	27.2
	Δ × w[n]	57	47	6	110	37.7
	w × Δ[o]	64	26	2	92	20.7
	Δ × Δ[p]	114	4	0	118	1.7
trp1-ade8	w × w[m]	63	18	0	81	11.1
	Δ × w[n]	89	20	1	110	11.8
	w × Δ[o]	77	14	1	92	10.9
	Δ × Δ[p]	115	3	0	118	1.3
ade6-fur1	w × w[q]	63	39	1	103	21.8
	w × Δ[r]	56	33	4	93	30.6
	Δ × w[s]	77	31	2	110	19.5
	Δ × Δ[t]	95	9	0	104	4.3
					Centromere linkage[u]	
ade6-lys1	w × w[q]	37	39	27	103	18.9
	w × Δ[r]	33	31	24	88	17.6
	Δ × w[s]	39	31	37	107	14.5
	Δ × Δ[t]	42	8	54	104	3.8

[a] w × w = wild × wild; w × Δ = wild × *dlc1Δ* × wild; Δ × w = *dlc1Δ* × wild; and Δ × Δ = *dlc1Δ* × *dlc1Δ*.
[b] Parental ditype.
[c] Tetratype.
[d] Nonparental ditype.
[e] HM101 × Z439-2A.
[f] F95-1A × Z439-2A.
[g] HM101 × F83-15A.
[h] F90-1D × F83-15A.
[i] HM101 × F131-1A.
[j] F90-1D × F132-1D.
[k] HM101 × F133-1A.
[l] F90-1D × F141-1C.
[m] F80-1B × Z439-2A.
[n] F84-5A × Z439-2A.
[o] F80-1B × F63-1C.
[p] F84-5A × F63-1C.
[q] L972 × F78-18A.
[r] L972 × F81-2D.
[s] F79-8A × F78-18A.
[t] F83-2A × F81-2D.
[u] Centromere linkage = total × 50.

and Table 6). In zygotic meiosis in the *dlc1* mutant, 20% of meiotic prophase nuclei contained two separated rDNA spots, of which one located near the SPB and the other located away from it (Figure 9, left). The loss of the heavy chain results in a similar defect (Yamamoto *et al.*, 1999). We repeated this experiment and 6 of 20 *dhc1-d2* zygotes had the

same abnormality in rDNA positioning. The *dlc1* mutation also affected the positioning of rDNA in azygotic meiosis. In more than a quarter of the cases, a single rDNA signal was located apart from the cluster of other telomeres (Figure 9, right, and Table 6). Telomere clusters are formed through relocation of telomeres toward the SPB that occurs shortly after the induc-

Table 4. Effect of the *dlc1* mutation on allelic versus ectopic recombination[a]

Spores produced from zygotic meioses were examined. Three independent experiments were performed. Ade[+] spores were produced from intragenic recombination between *ade6-469* and *ade6-M26* alleles.

	No. of Ade[+] spores per 10^5 viable spores		
Cross	exp. 1	exp. 2	exp. 3
Allelic			
Wild-type[b]	765	658	630
dlc1Δ[c]	52	63	58

	No. of Ade[+] spores/10^3 viable Leu[+] spores		
	exp. 1	exp. 2	exp. 3
Ectopic			
Wild-type[d]	52	46	44
dlc1Δ[e]	23	13	27

[a] Both alleles were on chromosome III (allelic) or *ade6-469* was on a plasmid, whereas *ade6-M26* was on chromosome III (ectopic).
[b] F154-4B × F155-1D.
[c] F156-2B × F153-1A.
[d] F154-7B.
[e] F156-3A.

tion to sexual phase, e.g., it occurs before nuclear fusion in zygotic meiosis (Chikashige *et al.*, 1997). Thus, the defective phenotype regarding the rDNA positioning might be most plausibly explained if the relocation process is affected by the *dlc1* mutation. Consistently, zygotes containing two haploid nuclei undergoing karyogamy, often contained rDNA at the tailing part of the nuclei, an abnormal configuration only rarely observed in wild-type nuclei (our unpublished data). It was not
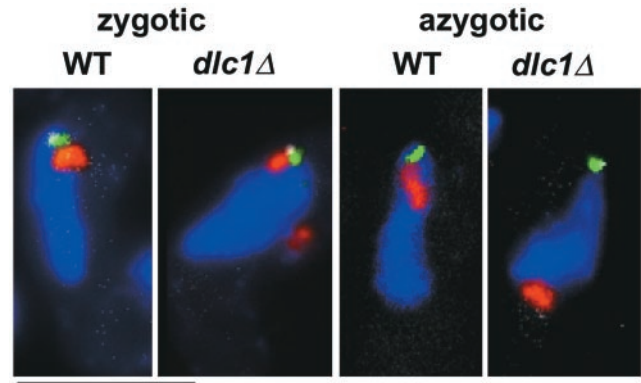
Figure 9. Defective rDNA relocation in the *dlc1Δ* mutant. Zygotic or azygotic meiotic prophase cells were stained with Cy5-rDNA (telomeres of chromosome III, red), Cy3-labeled cos212 (telomeres of chromosomes I and II, green), anti-Sad1 antibody (white), and DAPI (blue). The anti-Sad1 signal is closely associated with the cos212 signal in these figures. WT, Z310-10B; *dlc1Δ*, F52-3A. Bar, 10 μm.

determined, however, whether the problem of telomere relocation is specific for chromosomes III.

Both Karyogamy and Sporulation Were Partially Defective in dlc1 Mutant

The *dlc1* mutants had partially defective karyogamy and sporulation (Table 7). Because very few zygotes proceeded to meiosis I without nuclear fusion, it is likely that the higher incidence of unfused nuclei in the *dlc1* mutant zygotes was indicative of a delay in the nuclear fusion process. Experiments using the *mei1* mutant, which blocks entry into meiosis, supported this hypothesis (our unpublished data). The

Table 5. Random spore analysis of genetic linkage in *dlc1Δ*
Spores formed in zygotic and azygotic cells were analyzed for the linkage of two genetic markers.

	Cross	Number of colonies				Genetic distance (cM)[a]
Genetic markers		Ade[−]	Ade[+] Fur[−]	total Fur[−]	Fur[−]	
Zygotic	w × w[b]	1386	5361	6747	20.5	
	dlc1Δ × dlc1Δ[c]	108	4816	4924	2.2	
	dhc1-d4Δ × dhc1-d4Δ[d]	85	2679	2764	3.1	
	dlc1Δ dhc1-d4Δ × dlc1Δ dhc1-d4Δ[e]	229	50842	5107	0.4	
Azygotic	w/w[b]	130	1200	1330	9.8	
	dlc1Δ/dlc1Δ[c]	319	6311	6630	4.8	
	dhc1-d4Δ/dhc1-d4Δ[d]	93	1054	1147	8.1	
	dlc1Δ dhc1-d4Δ/dlc1Δ dhc1-d4Δ[e]	35	1435	1470	2.4	

[a] Ade[+] Fur[−]/total Fur[−] × 100.
[b] F109-2B × F109-2A.
[c] F96-2C × F96-2A.
[d] F170-1A × F171-1C.
[e] F168-1A × F169-1A. Only haploid colonies were scored.

Table 6. Positioning of telomeres in meiotic prophase nuclei

Type of meiosis	Telomere positioning	Wild-type[a]	dlc1Δ[a]
Zygotic	All telomeres clustered	75	40
	One of two rDNAs detached[b]	0	10
Azygotic	All telomeres clustered	83	37
	rDNA at the opposite end[b]	0	21

[a] Number of cells with indicated telomere configuration. Cells with clustered cos212 probe signal (telomeres of chromosomes I and II) were scored.

[b] See Figure 5.

delay in the nuclear fusion process was also consistent with a defect in karyogamy in the *dhc1* mutant (Yamamoto *et al.*, 1999). We next examined a *dlc1 dhc1* double mutant. In this strain both karyogamy and sporulation were impaired much more severely than in either of the single mutants (Table 7), consistent with the fact that these two genes are not involved in completely redundant functions as previously described for recombination.

Identification of Fission Yeast Gene Encoding a Homolog of 8-kDa Dynein Light Chain

In addition to the 14-kDa light chain homolog Dlc1, fission yeast carries a gene, which we named *dlc2⁺*, that encodes a protein highly homologous to the 8-kDa dynein light chain. We cloned and sequenced the *dlc2⁺* gene and determined the cDNA sequence as well. Dlc2 consisted of 85 amino acid

residues and its predicted molecular weight was 9.8 kDa. The sequence was 78% identical with that of the 8-kDa light chain in *D. melanogaster*. The *dlc2⁺* gene was transcribed during the vegetative phase and slightly induced in the sexual phase (Figure 2C). Dlc2 was tagged with GFP to examine its localization. As shown in Figure 10A, GFP-Dlc2 was enriched at the nuclear periphery. In meiotic prophase, the GFP signal was also abundant at the nuclear periphery, as well as near the SPB (Figure 10B). We then generated a *dlc2*-deleted allele and found that the *dlc2Δ* mutant did not have any notable defective phenotype in either the vegetative or the sexual phase, except that recombination frequency in zygotic meiosis was marginally reduced (for the *ade6-fur1* interval, it was three-fourths of the wild-type value). Thus, the 8-kDa dynein light chain is not essential in fission yeast.

DISCUSSION

The present study identified fission yeast genes *dlc1⁺* and *dlc2⁺* whose products had homology to the 14- and the 8-kDa dynein light chain family proteins, respectively. We were unable to detect any defective phenotypes associated with the loss of Dlc2. We observed a subtle effect on recombination in a *dlc2Δ* mutant, but the exact nature of the effect remains to be determined. Thus, we conclude that despite its high sequence homology to the 8-kDa proteins, and in contrast to other organisms, Dlc2 is not essential in the normal fission yeast life cycle. The localization of Dlc2 in the meiotic prophase partly overlaps with that of Dhc1/Dlc1. Therefore, it is possible that Dlc2 in this sexual phase exists in the dynein complex, but further study is needed to elucidate the significance of the colocalization.

Table 7. Karyogamy and spore formation in *dlc1Δ* and *dhc1Δ* zygotes
Cells were sporulated in MEB-Gal at 26°C for 24 h.

| Strain[a]	Karyogamy[b]	Spore formation[c]	Percentage of asci containing[d]				
			1	2	3	4	>4 spores
Zygotic							
Wild-type	90	84	0	1	0.5	99	0
dlc1Δ	55	81	11	30	8	51	0
dhc1Δ	44	71	9	20	10	58	3
kms1Δ	nd[e]	69	22	33	11	33	1
dlc1Δ dhc1Δ	3	47	49	33	10	7	0
dlc1Δ kms1Δ	nd	38	76	20	3	1	0
dhc1Δ kms1Δ	nd	68	28	27	16	29	0.5
Azygotic							
Wild-type		81	0	0	1	99	0
dlc1Δ		43	7	15	6	72	0
dhc1-d4Δ		62	1	3	6	90	0
dlc1Δ dhc1-d4Δ		27	23	32	13	31	0

[a] Strains used were Z310-10B (wild-type), F52-3A (*dlc1Δ*), F68-12B (*dhc1-d4*), Z121-4D (*kms1Δ*), F71-11D (*dlc1Δ kms1Δ*), F143-6B (*dlc1Δ dhc1-d4*), and F167-7B (*kms1Δ dhc1-d4*).

[b] Percentage of binucleated conjugants, but only those without a meiosis I spindle.

[c] Percentage of sporulated zygotes in total zygotes.

[d] More than 200 sporulated cells were counted.

[e] Not determined.
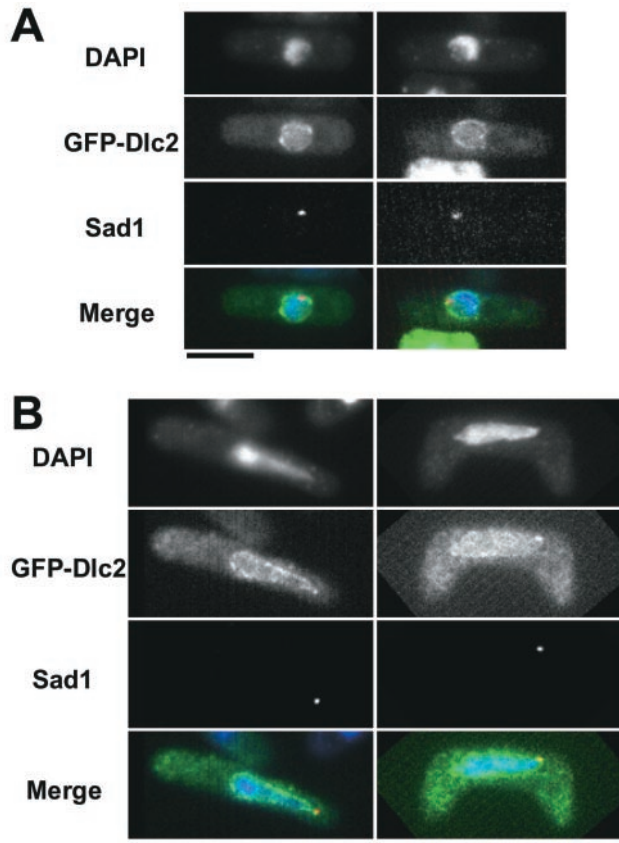
Figure 10. Localization of GFP-Dlc2. GFP-Dlc2 plasmid was introduced into a wild-type strain (Z310-10B) and fixed for microscopic observation. Merged: blue (DNA), green (GFP-Dlc2), and red (Sad1). (A) Vegetative cells. (B) Zygotes containing a horsetail nucleus. Bar, 5 μm.

Dlc1 is also not essential for vegetative growth, but it is required for several sexual processes in fission yeast. First, the *dlc1*Δ mutation affects dynein-dependent nuclear movement in the meiotic prophase; more specifically, the direction and duration of the nuclear movement are irregular. The mutation also brings about the displacement of Dhc1 from the microtubule anchors on the cortex and the failure in the formation of "directing microtubules" that would pull the SPB (Yamamoto *et al.*, 2001). In wild-type cells, the directing microtubules shorten from the distal ends in a coordinated manner with the SPB movement. After the SPB reaches the cell end, microtubules extend toward the opposite cell end to establish lateral binding with newly formed anchors so that the oscillatory movement will continue. Thus, the regular oscillatory nuclear movement appears to be ensured basically by the alternating assembly/disassembly of the dynein-containing anchors, although how this is achieved is not known (Yamamoto *et al.*, 2001). Results in the present study suggest that Dlc1 is required for the positioning and/or assembly of the anchors. One possibility is that Dlc1 is a component of cytoplasmic dynein complex and mediates binding to a cargo molecule on the cell cortex directly, as in the case of rhodopsin vesicles (Tai *et al.*, 1999),

or indirectly through interacting with the IC (Mok *et al.*, 2001). It cannot be ruled out, however, that Dlc1 has an indirect role in the localization of Dhc1; for example, Dlc1 might be required for the stability of the anchor or microtubules.

We demonstrated that the SPB movement in the *dlc1* mutant was still dependent on Dhc1. Therefore, a certain form of cytoplasmic dynein that lacks Dlc1 must be participating in the nuclear movement. Because some Dhc1 was present at the SPB, we tested one possibility that the sites of assembly/disassembly were changed from the distal ends to the proximal ends of the microtubules. This possibility was not supported by the bleaching experiment. The assembly/disassembly of microtubules occurred only at the distal ends in the *dlc1* mutant, similar to the *dhc1* mutant and wild-type cells. The rates of elongation/shortening of unfixed microtubules were not coordinated with the SPB motion. The SPB movement in the *dlc1* mutant was always accompanied by lengthening microtubules whose distal ends were fixed on the cell cortex. These facts strongly suggest that microtubules extending backward with fixed distal ends are at least partly responsible for the SPB movement in the *dlc1* mutant, although it could not be ruled out that unfixed microtubules somehow contribute to generate a force to drive the SPB. Microtubules with fixed distal ends might exist in wild-type cells, but their role in nuclear movement seems to be marginal compared with the prevailing pulling microtubules. Moreover, similarly fixed microtubules are present in a *dhc1* mutant and are engaged in residual nuclear movement (Yamamoto *et al.*, 2001). This suggests that Dhc1 is not involved in the fixation of the microtubular ends. At present, it is not known how Dhc1 or dynein are involved in the nuclear movement in the *dlc1* mutant. Dhc1 is noticeably present only at the SPB. It cannot be ruled out, however, that Dlc1 might be present at the fixed distal ends of microtubules on the cortex, although it must be in an amount too small to be detected. If this is the case, it is conceivable that Dhc1 enhances the elongation and/or stability of the microtubular ends and contributes to the nuclear movement in the *dlc1* mutant. Other factors that could influence nuclear motion, the nucleation at the SPB and the bundling of microtubules, might also be affected by Dhc1.

Another important finding in this study is that Dlc1 is required for efficient meiotic recombination. It has been argued that the horsetail nuclear movement is required for efficient meiotic recombination because recombination is reduced in *dhc1* mutants that lack nuclear movement (Yamamoto *et al.*, 1999; Yamamoto and Hiraoka, 2001). Although Dlc1 is related to Dhc1 and its loss brings about impaired nuclear movement, it is unlikely that the reduced recombination in the *dlc1* mutant is attributable solely to the problem in nuclear motion. The loss of Dlc1 function resulted in two- to threefold and 10-fold reduction in recombination frequency in azygotic and zygotic meiosis, respectively, in both wild-type and *dhc1* mutant background (Table 5). Importantly, the *dlc1 dhc1* double mutant completely lacked horsetail movement like in the *dhc1* single mutant, indicating that Dlc1 functions for efficient recombination even in the absence of nuclear movement and its function for recombination is at least partly independent of Dhc1. It is currently unknown why the lack of Dlc1 affects recombination. As shown in the present study, its effect was mainly on

homologous chromosome recombination but not on recombination between a plasmid and a chromosome; thus, it is probable that Dlc1 is required for efficient homologous chromosome pairing. Accordingly, relocation of rDNA, the marker of chromosome III telomeres, was impaired in the *dlc1* mutant. It remains to be addressed, however, whether the alignment of homologous chromosomes is actually affected by the mutation and also how Dlc1 is involved in the arrangement of chromosomes during the early phase of meiosis. In addition to the role in recombination, we found that Dlc1 is involved in karyogamy and sporulation in a Dhc1-independent manner. Because the SPB appears to be the only site of Dhc1-independent localization of Dlc1, we believe that such Dhc1-independent functions of Dlc1 are executed at the SPB. This notion will be addressed experimentally in future studies.

ACKNOWLEDGMENTS

REFERENCES

Bähler, J., Wu, J.Q., Longtine, M.S., Shah, N.G., McKenzie, A., Steever, A.B., Wach, A., Philippsen, P., and Pringle, J.R. (1998). Heterologous modules for efficient and versatile PCR-based gene targeting in *Schizosaccharomyces pombe*. Yeast *14*, 943–951.

Beckwith, S.M., Roghi, C.H., Liu, B., and Morris, R.N. (1998). The "8-kD" cytoplasmic dynein light chain is required for nuclear migration and for dynein heavy chain localization in *Aspergillus nidulans*. J. Cell Biol. *143*, 1239–1247.

Caggese, C., Moschetti, R., Ragone, G., Barsanti, P., and Caizzi, R. (2001). dtctex-1, the *Drosophila melanogaster* homolog of a putative murine t-complex distorter encoding a dynein light chain, is required for production of functional sperm. Mol. Genet. Genomics *265*, 436–444.

Chikashige, Y., Ding, D.-Q., Funabiki, H., Haraguchi, T., Mashiko, S., Yanagida, M., and Hiraoka, Y. (1994). Telomere-led premeiotic chromosome movement in fission yeast. Science *264*, 270–273.

Chikashige, Y., Ding, D.-Q., Imai, Y., Yamamoto, M., Haraguchi, T., and Hiraoka, Y. (1997). Meiotic nuclear reorganization: switching the position of centromeres and telomeres in the fission yeast *Schizosaccharomyces pombe*. EMBO J. *16*, 193–202.

Cooper, J.P., Watanabe, Y., and Nurse, P. (1998). Fission yeast Taz1 protein is required for meiotic telomere clustering and recombination. Nature *392*, 828–831.

Craven, R.A., Griffiths, D.J.F., Sheldrick, K.S., Randall, R.E., Hagan, I.M., and Carr, A.M. (1998). Vectors for the expression of tagged proteins in *Schizosaccharomyces pombe*. Gene *221*, 59–68.

Dick, T., Ray, K., Salz, H.K., and Chia, W. (1996). Cytoplasmic dynein (ddlc1) mutations cause morphogenetic defects and apoptotic cell death in *Drosophila melanogaster*. Mol. Cell. Biol. *16*, 1966–1977.

Ding, D.-Q., Chikashige, Y., Haraguchi, T., and Hiraoka, Y. (1998). Oscillatory nuclear movement in fission yeast meiotic prophase is driven by astral microtubules, as revealed by continuous observa-tion of chromosomes and microtubules in living cells. J. Cell Sci. *111*, 701–712.

Funabiki, H., Hagan, I., Uzawa, S., and Yanagida, M. (1993). Cell cycle-dependent specific positioning and clustering of centromeres and telomeres in fission yeast. J. Cell Biol. *121*, 961–976.

Hagan, I., and Yanagida, M. (1995). The product of the spindle formation gene *sad1*⁺ associates with the fission yeast spindle pole body and is essential for viability. J. Cell Biol. *129*, 1033–1047.

Haraguchi, T., Kaneda, T., and Hiraoka, Y. (1997). Dynamics of chromosomes and microtubules visualized by multi-wavelength fluorescence imaging in living mammalian cells: effects of mitotic inhibitors on cell cycle progression. Genes Cells *2*, 369–380.

Haraguchi, T., Koujin, T., Hayakawa, T., Kaneda, T., Tsutsumi, C., Imamoto, N., Akazawa, C., Sukegawa, J., Yoneda, Y., and Hiraoka, Y. (2000). Live fluorescence imaging reveals early recruitment of emerin, LBR, RanBP2, and Nup153 to reforming functional nuclear envelopes. J. Cell Sci. *113*, 779–794.

Hiraoka, Y. (1998). Meiotic telomeres: a matchmaker for homologous chromosomes. Genes Cells *3*, 405–413.

Karki, S., and Holzbaur, E.L. (1999). Cytoplasmic dynein and dynactin in cell division and intracellular transport. Curr. Opin. Cell Biol. *11*, 45–53.

King, S.M., Barbarese, E., Dillman, J.F., III, Patel-King, R.S., Carson, J.H., and Pfister, K.K. (1996a). Brain cytoplasmic and flagellar outer arm dyneins share a highly conserved *Mr* 8,000 light chain. J. Biol. Chem. *271*, 19358–19366.

King, S.M., Barbarese, E., Dillman, J.F., III, Benashski, S.E., Do, K.T., Patel-King, R.S., and Pfister, K.K. (1998). Cytoplasmic dynein contains a family of differentially expressed light chains. Biochemistry *37*, 15033–15041.

King, S.M., Dillman, J.F., III, Benashski, S.E., Lye, R.J., Patel-King, R.S., and Pfister, K.K. (1996b). The mouse *t*-complex-encoded protein Tctex-1 is a light chain of brain cytoplasmic dynein. J. Biol. Chem. *271*, 32281–32287.

Lader, E., Ha, H-S., O'Neill, M., Artzt, K., and Bennett, D. (1989). *tctex-1*: a candidate gene family for a mouse *t* complex sterility locus. Cell *58*, 969–979.

Miyata, M., Doi, H., Miyata, H., and Jonson, B.F. (1997). Sexual co-flocculation by heterothallic cells of the fission yeast *Schizosaccharomyces pombe* modulated by medium constituents. Antonie Leeuwenhoek *71*, 207–215.

Mizukami, T., Chang., W.I., Garkavtsev, I., Kaplan, N., Lombardi, D., Matsumoto, T., Niwa, O., Kounosu, A., Yanagida, M., Marr, T.G., and Beach, D. (1993). A 13 kb resolution cosmid map of the 14 Mb fission yeast genome by nonrandom sequence-tagged site mapping. Cell *73*, 121–132.

Mok, Y.K., Lo, K.W., and Zhang, M. (2001). Structure of Tctex-1 and its interaction with cytoplasmic dynein intermediate chain. J. Biol. Chem. *276*, 14067–14074.

Moreno, S., Klar, A., and Nurse, P. (1991). Molecular genetic analysis of the fission yeast *Schizosaccharomyces pombe*. Methods Enzymol. *194*, 795–823.

Nimmo, E.R., Pidoux, A.L., Perry, P.E., and Allshire, R.C. (1998). Defective meiosis in telomere-silencing mutants of *Schizosaccharomyces pombe*. Nature *392*, 825–828.

Niwa, O., Shimanuki, M., and Miki, F. (2000). Telomere-led bouquet formation facilitates homologous chromosome pairing and restricts ectopic interaction in fission yeast meiosis. EMBO J. *19*, 3831–3840.

Okajima, T., Tanabe, T., and Yasuda, T. (1993). Non-urea sodium dodecyl sulfate-polyacrylamide gel electrophoresis with high-molarity buffers for the separation of proteins and peptides. Anal. Biochem. *211*, 293–300.

Okazaki, K., Okayama, H., and Niwa, O. (2000). The polyubiquitin gene is essential for meiosis in fission yeast. Exp. Cell Res. *254*, 143–152.

Pazour, G.J., Wilkerson, C.G., and Witman, G.B. (1998). A dynein light chain is essential for the retrograde particle movement of intraflagellar transport (IFT). J. Cell Biol. *141*, 979–992.

Phillis, R., Statton, D., Caruccio, P., and Murphey, R.K. (1996). Mutations in the 8 kDa dynein light chain gene disrupt sensory axon projections in the *Drosophila* imaginal CNS. Development *122*, 2955–2963.

Ponticelli, A.S., and Smith, G.R. (1989). Meiotic recombination-deficient mutants of *Schizosaccharomyces pombe.* Genetics *123*, 45–54.

Shimanuki, M., Miki, F., Ding, D.-Q., Chikashige, Y., Hiraoka, Y., Horio, T., and Niwa, O. (1997). A novel fission yeast gene, *kms1$^+$*, is required for the formation of meiotic prophase-specific nuclear architecture. Mol. Gen. Genet *254*, 238–249.

Silve, S., Volland, C., Garnier, C., Jund, R., Chevallier, M.R., and Haguenauer-Tsapis, R. (1991). Membrane insertion of uracil permease, a polytopic yeast plasma membrane protein. Mol. Cell. Biol. *11*, 1114–1124.

Tai, A.W., Chuang, J.Z., Bode, C., Wolfrum, U., and Sung, C.H. (1999). Rhodopsin's carboxy-terminal cytoplasmic tail acts as a membrane receptor for cytoplasmic dynein by binding to the dynein light chain Tctex-1. Cell *97*, 877–887.

Tai, A.W., Chuang, J.Z., and Sung, C.H. (1998). Localization of Tctex-1, a cytoplasmic dynein light chain, to the Golgi apparatus and evidence for dynein complex heterogeneity. J. Biol. Chem. *273*, 19639–19649.

Tai, A.W., Chuang, J.Z., and Sung, C.H. (2001). Cytoplasmic dynein regulation by subunit heterogeneity and its role in apical transport. J. Cell Biol. *153*, 1499–1509.

Tanaka, H., Tanaka, K., Murakami, H., and Okayama, H. (1999). Fission yeast *cdc24* is a replication factor C- and proliferating cell nuclear antigen-interacting factor essential for S-phase completion. Mol. Cell. Biol. *19*, 1038–1048.

Tanaka, K., Yonekawa, T., Kawasaki, Y., Kai, M., Furuya, K., Iwasaki, M., Murakami, H., Yanagida, M., and Okayama, H. (2000). Fission yeast Eso1p is required for establishing sister chromatid cohesion during S phase. Mol. Cell. Biol. *20*, 3459–3469.

Tange, Y., Horio, T., Shimanuki, M., Ding, D.-Q., Hiraoka, Y., and Niwa, O. (1998). A novel fission yeast gene *tht1$^+$*, is required for the fusion of nuclear envelopes during karyogamy. J. Cell Biol. *140*, 247–258.

Toda, T., Nakaseko, Y., Niwa, O., and Yanagida, M. (1984). Mapping of rRNA genes by integration of hybrid plasmids in *Schizosaccharomyces pombe.* Curr. Genet. *8*, 93–97.

Yamamoto, A., and Hiraoka, Y. (2001). How do meiotic chromosomes meet their homologous partners?: lessons from fission yeast. BioEssays *23*, 526–533.

Yamamoto, A., Tsutsumi, C., Kojima, H., Oiwa, K., and Hiraoka, Y. (2001). Dynamic behavior of microtubules during dynein-dependent nuclear migration of meiotic prophase in fission yeast. Mol. Biol. Cell *12*, 3933–3946.

Yamamoto, A., West, R.R., McIntosh, J.R., and Hiraoka, Y. (1999). A cytoplasmic dynein heavy chain is required for oscillatory nuclear movement of meiotic prophase and efficient meiotic recombination in fission yeast. J. Cell Biol. *145*, 1233–1249.